JACS
JOURNAL OF THE AMERICAN CHEMICAL SOCIETY
pubs.acs.org/JACS
Article

Metal Ion and Guest-Mediated Spontaneous Resolution and Solvent-Induced Chiral Symmetry Breaking in Guanine-Based Metallosupramolecular Networks

Antonino Cucinotta, Christophe Kahlfuss, Andrea Minoia, Samuel Eyley, Keanu Zwaenepoel, Gangamallaiah Velpula, Wim Thielemans, Roberto Lazzaroni, Véronique Bulach, Mir Wais Hosseini, Kunal S. Mali,* and Steven De Feyter*

Cite This: *J. Am. Chem. Soc.* 2023, 145, 1194–1205

ABSTRACT: Two-dimensional (2D) chirality has been actively studied in view of numerous applications of chiral surfaces such as in chiral resolutions and enantioselective catalysis. Here, we report on the expression and amplification of chirality in hybrid 2D metallosupramolecular networks formed by a nucleobase derivative. Self-assembly of a guanine derivative appended with a pyridyl node was studied at the solution-graphite interface in the presence and absence of coordinating metal ions. In the absence of coordinating metal ions, a monolayer that is representative of a racemic compound was obtained. This system underwent spontaneous resolution upon addition of a coordinating ion and led to the formation of a racemic conglomerate. The spontaneous resolution could also be achieved upon addition of a suitable guest molecule. The mirror symmetry observed in the formation of the metallosupramolecular networks could be broken *via* the use of an enantiopure solvent, which led to the formation of a globally homochiral surface.

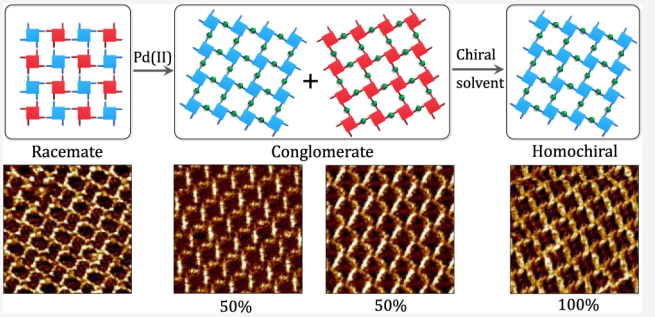

INTRODUCTION

Metal–organic coordination is ubiquitous in biology and materials. Thanks to the reversible, highly directional, and predictable nature of the dative bond, coordination-driven self-assembly has been widely exploited as a bottom-up strategy for the fabrication of a variety of materials ranging from discrete metallosupramolecular architectures[1,2] to metallosupramolecular polymers[3] and from two-dimensional (2D) metal–organic coordination networks (MOCNs)[4,5] to metal–organic frameworks (MOFs).[6,7] These hybrid organic–inorganic materials have attracted substantial attention in view of their remarkable properties and numerous potential applications.[1−7]

MOFs consist of infinitely extended porous networks with crystalline arrangement of organic ligands held together by suitable metal nodes giving rise to permanent porosity. The advent of graphene and related inorganic 2D materials has fueled the research on 2D analogues of such hybrid organic–inorganic systems in search of diversity in structure and properties. In fact, the synthesis of layered MOFs or so-called 2D-MOFs is an emerging area of research with significant focus on the exploration of their properties. Since the modular design of 2D-MOFs allows construction of structures with tailored properties, the mechanical, electrical, optical, opto-electronic, magnetic, and catalytic properties of layered 2D-MOFs are under intense scrutiny.[8,9]

Metallosupramolecular systems have been traditionally characterized using different techniques depending on the dimensionality of the material. Discrete metallosupramolecular assemblies such as 2D metallacycles, higher-order supramolecules and metal–organic cages are characterized using multidimensional NMR and mass spectrometry (MS),[10] whereas powder X-ray diffraction (PXRD) serves as a primary tool for the characterization of MOFs, which are typically isolated as insoluble crystalline powders.[7] Single-crystal structures of a MOF have also been elucidated using X-ray diffraction.[11] Recent years have witnessed increasing use of electron microscopy for the characterization of both the discrete systems[12,13] and framework materials.[11,14,15]

Surface-confined MOCNs are typically characterized using scanning probe methods, especially scanning tunneling

Received: October 15, 2022
Published: December 28, 2022

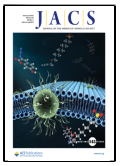

https://doi.org/10.1021/jacs.2c10933
J. Am. Chem. Soc. 2023, 145, 1194–1205

Scheme 1. Schematic Showing the Molecular and Supramolecular Design Strategy Employed in This Work[a]

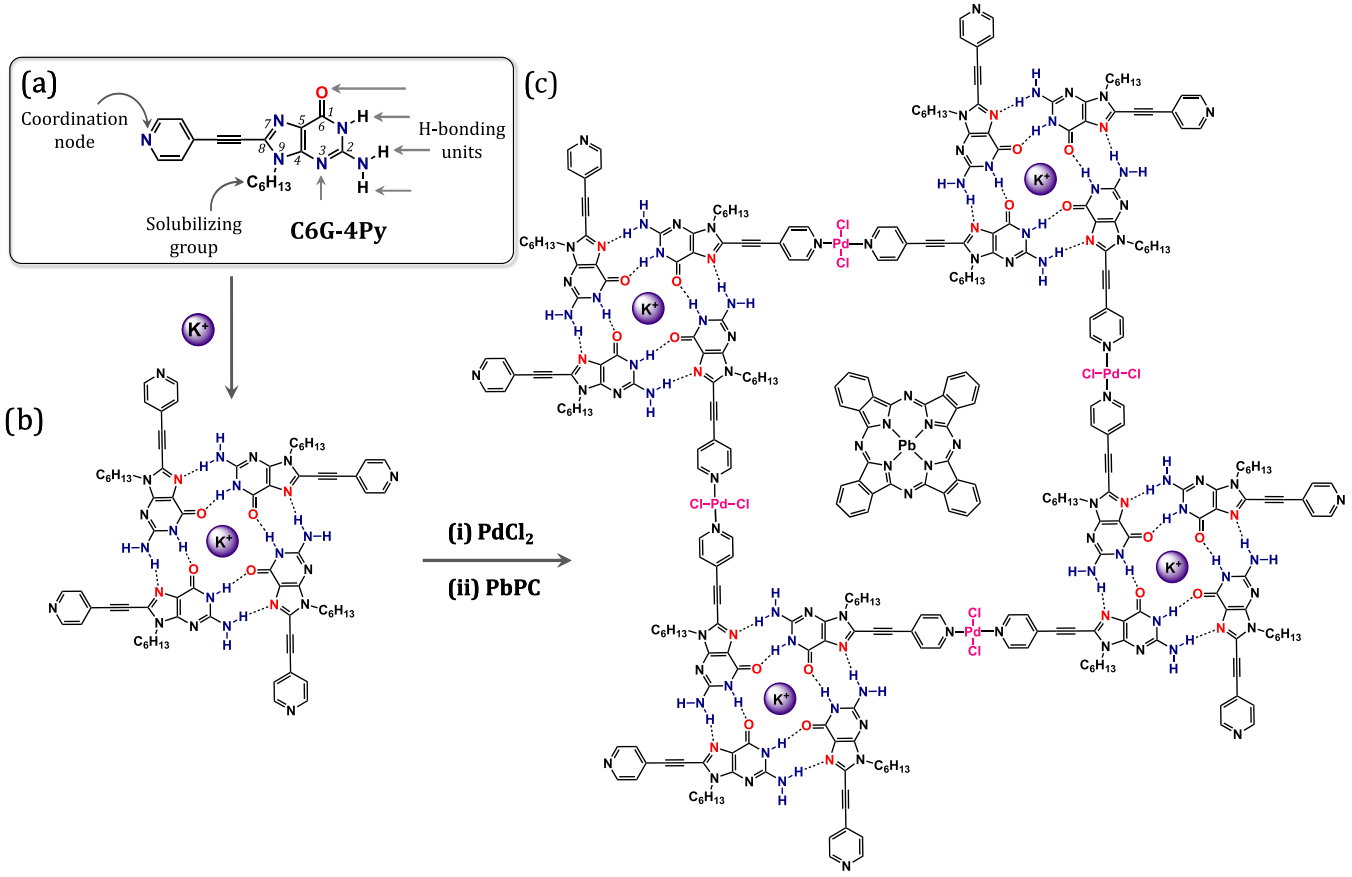

[a](a) Molecular structure of **C6G-4Py**. (b) Cation templated G-quartet formation. (c) Self-assembly of the H-bonded G-quartets through metal coordination at the pyridyl site of the tectons followed by immobilization of a guest molecule (lead phthalocyanine) within its cavities.

microscopy (STM).[16,17] STM images provide unprecedented resolution while revealing several structural aspects including the nature and the extent of defects that often go unnoticed in ensemble measurements. While STM can be carried out both under ultrahigh vacuum (UHV) conditions and at the solution−solid interface, the former dominates the literature.[16,17] There exist only a few reported examples of one-dimensional (1D) and 2D MOCNs constructed and characterized at the solution−solid interface.[18−21] Despite the challenges associated with STM imaging in the presence of metal-ion solutions, STM characterization of MOCNs at the solution−solid interface at room temperature is valuable as it provides insight into the dynamical aspects of MOCN formation. STM has also been employed for the characterization of discrete metallosupramolecules.[22−24] Thin films of MOCNs[25,26] have been investigated using atomic force microscopy (AFM), and single-layered MOCNs have been imaged at molecular resolution using non-contact AFM.[27]

An important structural facet of metallosupramolecular systems that has received considerable attention in the recent past is their chirality. Chirality is an all-pervasive structural feature found in the materials and the biological world. Obtaining chiral (enantiopure) materials is highly desired for metal−organic systems as well in view of potential applications in chiral recognition, separation, and catalysis.[28,29] Similarly, chirality of surface-confined (metallo)supramolecular networks is a highly researched domain that continues to flourish. A study of the so-called "2D chirality" provides insight into the molecular mechanisms governing the expression, induction, and amplification of chirality on surfaces under well-defined conditions. As a bottom-up strategy, the on-surface self-assembly approach not only enables the fabrication of low-dimensional (homo)chiral nanostructures but also allows controlling the structure of homochiral films/surfaces *via* rational design strategies.[30−32]

Analogous to MOFs[29] and discrete metallosupramolecular systems,[28] induction of chirality in surface-confined supramolecular networks can be achieved using the "hard" or the "soft" approach.[28] The former employs enantiopure building blocks to obtain a pre-defined handedness where the organic ligands are chiral even in the absence of metal coordination.[17] The latter, on the other hand, uses achiral building blocks that, upon metal coordination and surface confinement, achieve discrete chirality,[33,34] which will be lost upon desorption and/or demetallation. The chirality of surface-confined MOCNs has been studied for systems investigated using UHV-STM.[17,35] To the best of our knowledge, there exist no reports describing the expression/induction of chirality in metallosupramolecular networks fabricated and characterized at the solution−solid interface. Nevertheless, the 2D chirality of metal-free self-assembled molecular networks (SAMNs) has been intensively studied at the solution−solid interface.[31] These studies indicate that chirality is readily achieved upon confinement in 2D. Even prochiral molecules assemble into chiral domains due to the loss of symmetry elements upon surface confinement. The surface, however, remains globally

https://doi.org/10.1021/jacs.2c10933
J. Am. Chem. Soc. 2023, 145, 1194−1205

Scheme 2. Successive Chiral Transitions within the Metallosupramolecular Networks Formed by C6G-4Py at the Solution–Solid Interface[a]

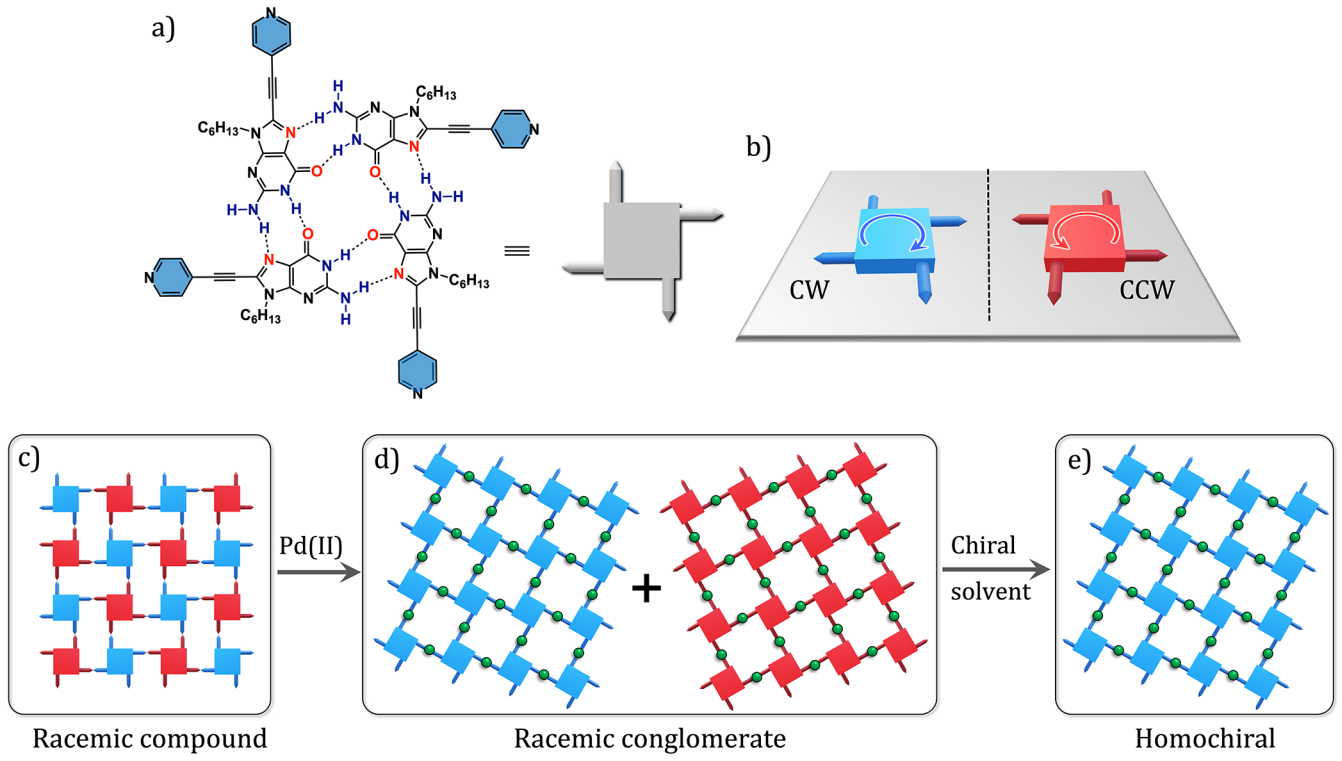

[a](a, b) Schematic illustrating the prochiral nature of the G-quadruplex and how, upon surface adsorption, two types of G-quartets differing in their handedness, namely, clockwise (CW) and counterclockwise (CCW), can be formed. (c) Self-assembly of **C6G-4Py** at the solution–solid interface leads to the formation of a racemic compound where both the CW and CCW G-quartets are present in a periodic manner. (d) Addition of Pd(II) leads to a distinct change in the network structure resulting in the formation of a racemic conglomerate where the CW and CCW quartets are now separated in different domains. (e) When **C6G-4Py** self-assembles at the interface between a chiral solvent and graphite, a homochiral network is obtained with preferential formation of either CW or CCW domains of G-quartets.

racemic due to the equal surface coverage of opposite-handed domains.

Various strategies have been employed for breaking the mirror symmetry observed in SAMNs of prochiral molecules. The "sergeants-and-soldiers" principle, where a small amount of structurally similar enantiopure dopant is merged in the SAMNs formed by an achiral building block to force the latter into a homochiral assembly defined by the handedness of the former, remains an important strategy.[36,37] For enantiopure building blocks, a small enantiomeric excess of one enantiomer has been used to suppress the chiral expression of the other in a so-called "majority rules" approach.[38,39] Magnetic field has also been used for breaking the mirror symmetry in SAMNs of liquid crystals.[40] We have pioneered the solvent-mediated chirality transfer approach[41] where network formation from an enantiopure solvent leads to the emergence of homochirality in the SAMNs.[42−44] This type of chiral amplification is a generic strategy that is uniquely applicable to the solution–solid interface and circumvents the tedious synthesis of structurally similar enantiopure "sergeants" needed in the "sergeants-soldiers" approach.

In this work, we report on the expression and amplification of chirality in hierarchically complex metallosupramolecular networks formed by a nucleobase derivative. The latter was achieved using chirality transfer from an enantiopure solvent. The self-assembly of a guanine derivative appended with an ethynyl-4-pyridyl moiety (**C6G-4Py**, Scheme 1a), in the presence and absence of metal ions was studied at the heptanoic acid-graphite interface. We report on the self-assembly of **C6G-4Py** into hydrogen-bonded guanine quartets (G-quartets) in the presence and absence of potassium ions. The G-quartets could be further connected at the pyridyl nodes *via* coordination to Pd(II) yielding an extended hybrid metallosupramolecular network stabilized by H-bonding and metal coordination. The porous network with square-shaped cavities was used for immobilizing molecular guests (Scheme 1). More importantly, we discuss the expression of chirality in each step and how the system undergoes changes in the chiral composition upon addition of metal ions and/or guest molecules. The SAMN represents a racemic compound in the absence of coordinating Pd(II); however, it evolves into a racemic conglomerate upon coordination to Pd(II) and then further becomes homochiral when the assembly is carried out from an enantiopure chiral solvent. Plausible reasons behind the successive chiral transitions are discussed.

RESULTS AND DISCUSSION

Design of the Hybrid Metallosupramolecular Network. The metallosupramolecular network is designed to be stabilized *via* multivalent interactions comprising hydrogen-bonding and metal–organic coordination.[45,46] Guanine was used as the central motif in the design as it is one of the most studied nucleobases. It offers self-complementary hydrogen-bonding sites that give rise to a variety of supramolecular

https://doi.org/10.1021/jacs.2c10933
J. Am. Chem. Soc. 2023, 145, 1194−1205

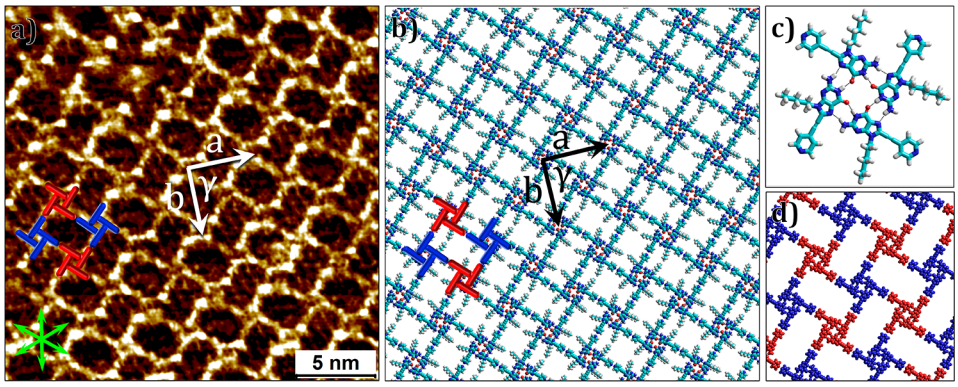

Figure 1. Self-assembly of **C6G-4Py** at the heptanoic acid−graphite interface in the absence of added metal ions. (a) High-resolution STM image of the self-assembled network of **C6G-4Py**. The opposite-handed G-quadruplexes are highlighted in blue (CW) and red (CCW). The unit cell parameters are: $a = 3.9 \pm 0.1$ nm, $b = 3.9 \pm 0.1$ nm, $\gamma = 90 \pm 1°$. Imaging parameters: $I_{set} = 70$ pA, $V_{bias} = -1.2$ V. [**C6G-4Py**] $= 2.5 \times 10^{-4}$ M. The graphite symmetry axes (green arrows) are displayed in the lower left corner. (b) Molecular model corresponding to the self-assembled network built using the lattice parameters obtained from calibrated STM images. (c) Molecular model for the G-quadruplex in the presence of a K^+ ion. (d) Molecular model showing the crystalline arrangement of CW (blue) and CCW (red) G-quadruplexes within the self-assembled network, which represents a racemic compound. For large-scale STM images, see Figure S1 in the Supporting Information.

Table 1. Unit Cell Parameters of the Different Supramolecular Networks

	unit cell				
system	a (nm)	b (nm)	γ (deg)	plane group	chiral composition
C6G-4Py	3.9 ± 0.1	3.9 ± 0.1	90.0 ± 1.0	*p4gm*	racemic compound
C6G-4Py/Pd(II)	2.9 ± 0.1	2.9 ± 0.1	90.0 ± 1.0	*p4*	racemic conglomerate
C6G-4Py/PbPc	2.9 ± 0.1	2.9 ± 0.1	89.0 ± 1.0	*p4*	racemic conglomerate
C6G-4Py/Pd(II)/CA[a]	2.9 ± 0.1	2.9 ± 0.1	90.0 ± 1.0	*p4*	homochiral

[a]Measurement carried out in (*R*)-(+)-citronellic acid. All other entries correspond to measurements carried out in heptanoic acid.

architectures. Guanine derivatives can self-assemble into dimers, ribbons, or tetramers depending on the precise experimental conditions.[47] The H-bonded tetramers, also known as G-quartets or tetrads, have been widely studied in solution, in the solid state,[48] and also as monolayers on solid surfaces.[49,50] They are formed *via* a quasi-planar association of four guanine units linked by a network of eight cooperative hydrogen bonds. G-quadruplexes, on the other hand, are secondary structures formed *via* the association of a minimum of two G-quartets by $\pi-\pi$ stacking and coordination to a monovalent cation.

Scheme 1a shows the molecular structure of **C6G-4Py**, which consists of a guanine unit appended with an ethynyl-4-pyridyl moiety at the C-8 position. We anticipated that the H-bonding groups will lead to the formation of G-quartets templated by monovalent cations such as potassium (K^+) (Scheme 1b). The G-quartets are further expected to be held together at the pyridyl node *via* an appropriate metal ion such as Pd(II), which can coordinate two ligands through nitrogen atoms in a linear geometry leading to the formation of an extended 2D porous network stabilized *via* H-bonding interactions at the quartet level and *via* metal−organic coordination at the pyridyl nodes (Scheme 1c).[51] To improve the solubility of the building block, an *n*-hexyl chain was introduced at the N-9 position. Moreover, given the porosity of the resulting network, we envisioned that the pores could be used for the immobilization of guest molecules such as metal phthalocyanines giving rise to a hierarchically complex multicomponent system (Scheme 1c). The overall (supra)-molecular design counts on recognition between appropriate functional groups while avoiding competitive H-bonding and metal−ligand interactions.[51]

Scheme 2a,b highlights the expression of chirality at the level G-quartets of **C6G-4Py** upon confinement against a solid surface. We define the handedness of the quartet by looking at the ethynyl-4-pyridyl "arms" as clockwise (CW, blue) or counterclockwise (CCW, red), as depicted in Scheme 2b. The chiral composition of all systems studied in this work was defined on the basis of this characterization of handedness. The chirality of the metallosupramolecular network changes significantly (*vide infra*) upon the addition of metal ions and/or guest molecules (Scheme 2c,d) and one out of two possible enantiomorphous domains could be selected to obtain a homochiral surface by carrying out the self-assembly from an enantiopure chiral solvent (Scheme 2e).

Fabrication of the Metallosupramolecular Networks at the Solution−Solid Interface. Heptanoic acid was used as the solvent for initial STM experiments. It was chosen due to its ability to dissolve **C6G-4Py** at reasonable concentrations, its high vapor pressure, and lower tendency to compete for the surface compared to higher alkanoic acids such as octanoic or nonanoic acid.[52] Figure 1a shows a high-resolution STM image of the supramolecular network formed by **C6G-4Py** at the heptanoic acid-graphite interface. In the absence of any added metal ions, **C6G-4Py** forms a porous network with rectangular cavities. We attribute the bright rims of the porous network to the pyridyl-appended guanine backbone, whereas the short *n*-hexyl chains are not resolved. The vertices of each rectangular cavity are made up of the H-bonded G-quartet (Figure 1c) and the distance between two adjacent quartets is 2.8 ± 0.1 nm. A careful observation of the STM image revealed that the arms

https://doi.org/10.1021/jacs.2c10933
J. Am. Chem. Soc. 2023, 145, 1194−1205

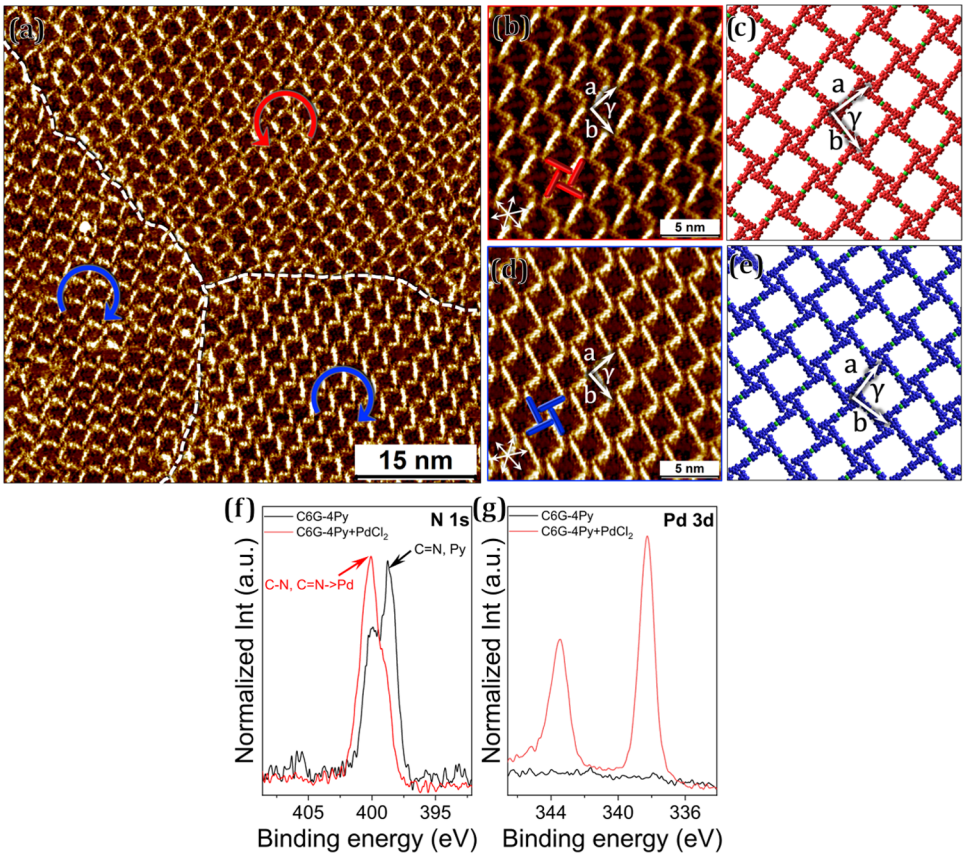

Figure 2. Self-assembly of **C6G-4Py** at the heptanoic acid−graphite interface in the presence of added Pd(II) in the form of $PdCl_2$. [**C6G-4Py**] = [$PdCl_2$] = 1.0×10^{-4} M. Solvent: heptanoic acid/DMSO = 99:1 mixture. (a) Large-scale image showing the formation of enantiomorphous domains. The handedness of the G-quartets is domain-specific. Domains containing CW (blue) and CCW (red) G-quadruplexes are indicated. (b, c) High-resolution STM image and proposed molecular model for the CCW domain. (d, e) High-resolution STM image and proposed molecular model for the CCW domain. The unit cell parameters for the CW and CCW domains are virtually identical: $a = 2.9 \pm 0.1$ nm, $b = 2.9 \pm 0.1$ nm, $\gamma = 90 \pm 1°$. Imaging parameters: (a) $I_{set} = 180$ pA, $V_{bias} = -380$ mV, (b) $I_{set} = 150$ pA, $V_{bias} = -350$ mV. (f, g) High-resolution XPS spectra showing the N 1s and Pd 3d regions.

emanating from each vertex are slightly offset with respect to each other, which can be explained by considering the opposite handedness for adjacent quartets. The CW and CCW G-quartets are highlighted with blue- and red-colored structures, respectively in Figure 1.

The equal stoichiometry and the crystalline ordering of the CW and CCW quartets make this structure a racemic compound or a racemate.[32,53] The rectangular cavities of the network reveal striped contrast, which could possibly arise due to the *n*-hexyl chains and/or co-adsorbed heptanoic acid molecules. A molecular model based on calibrated STM data is presented in Figure 1b, which clearly reveals open spaces within the network that could be occupied by heptanoic acid molecules. An additional molecular model, where the *n*-hexyl chains have been omitted for the sake of clarity, reproduces the symmetry of the rectangular network observed in the STM image (Figure 1d). Given the racemic nature of the network, the unit cell vectors do not correspond to the distance between adjacent G-quartets (Table 1) but rather to the distance between G-quartets with the same handedness (Figure 1d). The unit cell belongs to *p4gm* plane group. Note that a porous self-assembled network was obtained even in the absence of alkali metals such as Na^+ or K^+, which are known to template the formation of G-quadruplexes. Nevertheless, guanine derivatives are known to form G-quadruplexes even in the absence of alkali metals.[54]

Addition of a DMSO solution of KCl to introduce K^+ ions into the system resulted in no change in the self-assembled network. The unit cell remains the same in the presence of added K^+ ions (Figure S2 in the Supporting Information); however, the STM imaging of the monolayer became challenging in view of increased faradic current. X-ray photoelectron spectroscopy (XPS) analysis (*vide infra*) of the monolayers formed in the absence of any added metal ions revealed trace amounts of Na^+ present on the surface (Figure S3 in the Supporting Information); however, the amount of trace Na^+ appears to be too low to template G-quartet formation across the entire surface. Thus, we conclude that the supramolecular network presented in Figure 1 is obtained even in the absence of the templating effect of alkali metals.[54] The formation of a racemic compound in the present case is not entirely unusual since prochiral molecules are known to form racemic as well as conglomerate monolayers.[32,55]

Pd(II) was chosen to investigate the coordination chemistry of **C6G-4Py** due to its affinity toward nitrogen and its coordination geometry. $PdCl_2$ forms adducts with Lewis base ligands, resulting in square planar complexes in which two trans positions are occupied by chloride anions and the other two positions accommodate the Lewis bases. The metal salt was dissolved in DMSO and added to the **C6G-4Py** solution in heptanoic acid to form 1:1 mixtures of the ligand and the metal. Figure 2a shows a large-scale STM image of the SAMN

https://doi.org/10.1021/jacs.2c10933
J. Am. Chem. Soc. 2023, 145, 1194−1205

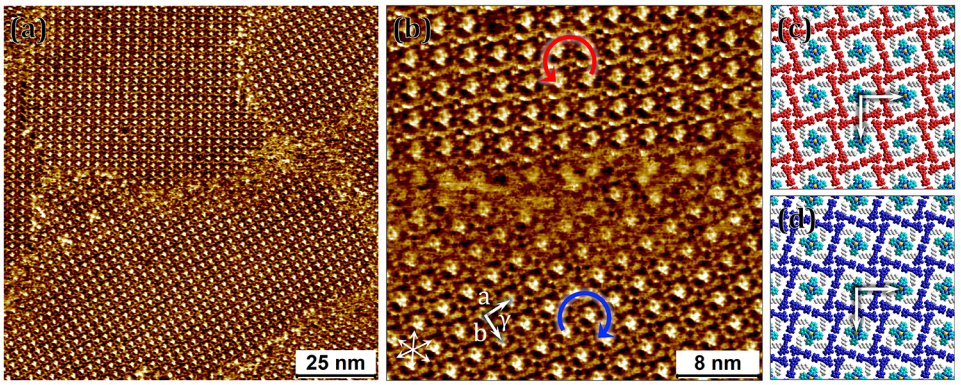

Figure 3. Self-assembly of **C6G-4Py** at the heptanoic acid-HOPG interface in the presence of PbPc. [**C6G-4Py**] = [PbPc] = 2.5×10^{-4} M. (a) Large-scale STM image showing the host−guest network in which PbPc is immobilized within the square-shaped cavities formed by **C6G-4Py**. (b) Small-scale STM image showing two domains containing CW (blue arrow) and CCW (red arrow) G-quartets indicating the formation of a racemic conglomerate. (c, d) Tentative molecular models depicting the structure of the host−guest network in the case of CCW and CW domains, respectively. The *n*-hexyl chains are colored white, and the rest of the **C6G-4Py** in blue (CW) or red (CCW) for the sake of clarity. Imaging parameters: (a, b) I_{set} = 80 pA, V_{bias} = −400 mV.

obtained from a premixed solution containing **C6G-4Py** and Pd(II) at the heptanoic acid−graphite interface. In contrast to the racemic network obtained in the absence of Pd(II), which is characterized by rectangular cavities (see Figure 1a), the STM image in Figure 2a shows a network with square-shaped cavities clearly indicating a change in the network structure upon binding to Pd(II). While the network is still composed of the same fundamental motif, namely, the G-quartets, a major change occurred in the chiral composition of the system. Addition of Pd(II) to the system caused spontaneous resolution, leading to the formation of separate domains of CW (blue arrow, Figure 2a) and CCW (red arrow, Figure 2a) G-quartets. Such conglomerate crystallization remains a critical step for deracemization protocols used in the bulk.[56] Figure 2b−e shows high-resolution STM images of the enantiomorphous domains and the corresponding proposed molecular models, respectively. We hypothesize that the G-quartets in each enantiomorphous domain are held together *via* coordination of the pyridyl nodes to Pd(II). The STM images do not show an obvious contrast at the metal−ligand junction; however, a significant change in the size of the unit cell and the chiral composition clearly implies the incorporation of Pd(II) in the self-assembling system (Table 1). Our density functional theory (DFT) calculations show that the lowest unoccupied molecular orbital (LUMO) of the metal-coordinated dimer of **C6G-4Py**, which is responsible for the molecular contrast seen in the STM images, is mostly localized on the two **C6G-4Py** molecules, with only a minor contribution from the metal center (Figure S8 in the Supporting Information). The distance between two adjacent quartets is 2.9 ± 0.1 nm, and it corresponds to the unit cell vector as the G-quartets within a given domain have the same handedness. The unit cell belongs to chiral plane group *p*4.

To unambiguously confirm the coordination of Pd(II) to the pyridinic nitrogen sites of **C6G-4Py** within the SAMNs, the as-formed monolayers were dried and subjected to detailed XPS analysis (see Section S2, Supporting Information). Figure 2f shows the nitrogen 1s region for the monolayer of **C6G-4Py** physisorbed on highly oriented pyrolytic graphite (HOPG). The peak (gray) shows two maxima at 398.7 and 400.2 eV. The lower binding energy peak is due to a combination of contributions from C═N environments in guanine,[57] and the pyridyl nitrogen (C═N, Py), while the higher binding energy environment is due to C−N environments in the guanine moiety. Following the treatment with $PdCl_2$, retention of Pd(II) by the SAMN is confirmed by the Pd $3d_{5/2}$ peak at 338.3 eV (Figure 2g, red). Additionally, there is a significant reduction in the relative intensity of the lower binding energy peak in the nitrogen 1s spectrum (Figure 2f, red). This can be ascribed to coordination of the palladium by either the pyridinyl or guanine C═N species and is consistent with shifts in nitrogen 1s binding energy reported in the literature for the formation of pyridine complexes of palladium(II), which would result in the overlap of the Pd−N environment with that from remaining C−N in the structure.[58]

Despite the confirmation of coordination of the nitrogen sites to palladium, it was not possible to unambiguously ascertain whether coordination of Pd(II) occurs selectively at the pyridyl node or also to the guanine nitrogen. In fact, based on quantification of the survey scan data (see Figure S3 and Table S1 in the Supporting Information), there is significantly more palladium than would be expected from coordination of the pyridine moieties alone, which may indicate binding to additional nitrogen sites within the molecular framework.

Comparison of the molecular densities of the networks reveals that the one formed in the absence of added Pd(II) is denser (0.53 molecules/nm^2) compared to the metallosupramolecular network obtained upon coordination to Pd(II) (0.48 molecules/nm^2). While this difference may appear rather small, it is well known that seemingly small differences in molecular densities per unit area in the case of self-assembled monolayers are often decisive in the selection of one structure over the other.[59] This observation is in line with the Wallach rule,[60] which states that racemic crystals are often denser than the corresponding enantiopure ones. In the present case, the metallosupramolecular network, which represents a racemic conglomerate, can be considered enantiopure at the level of single domains and hence qualifies the Wallach rule in being less dense than the racemic compound obtained in the absence of Pd(II). However, we note that Wallach's original correlation was based on a limited set of nine compounds. Later studies have shown that although there may exist a small difference in the densities of the racemates and conglomerates, there exist a number of systems where the Wallach rule does not apply.[61]

https://doi.org/10.1021/jacs.2c10933
J. Am. Chem. Soc. 2023, 145, 1194−1205

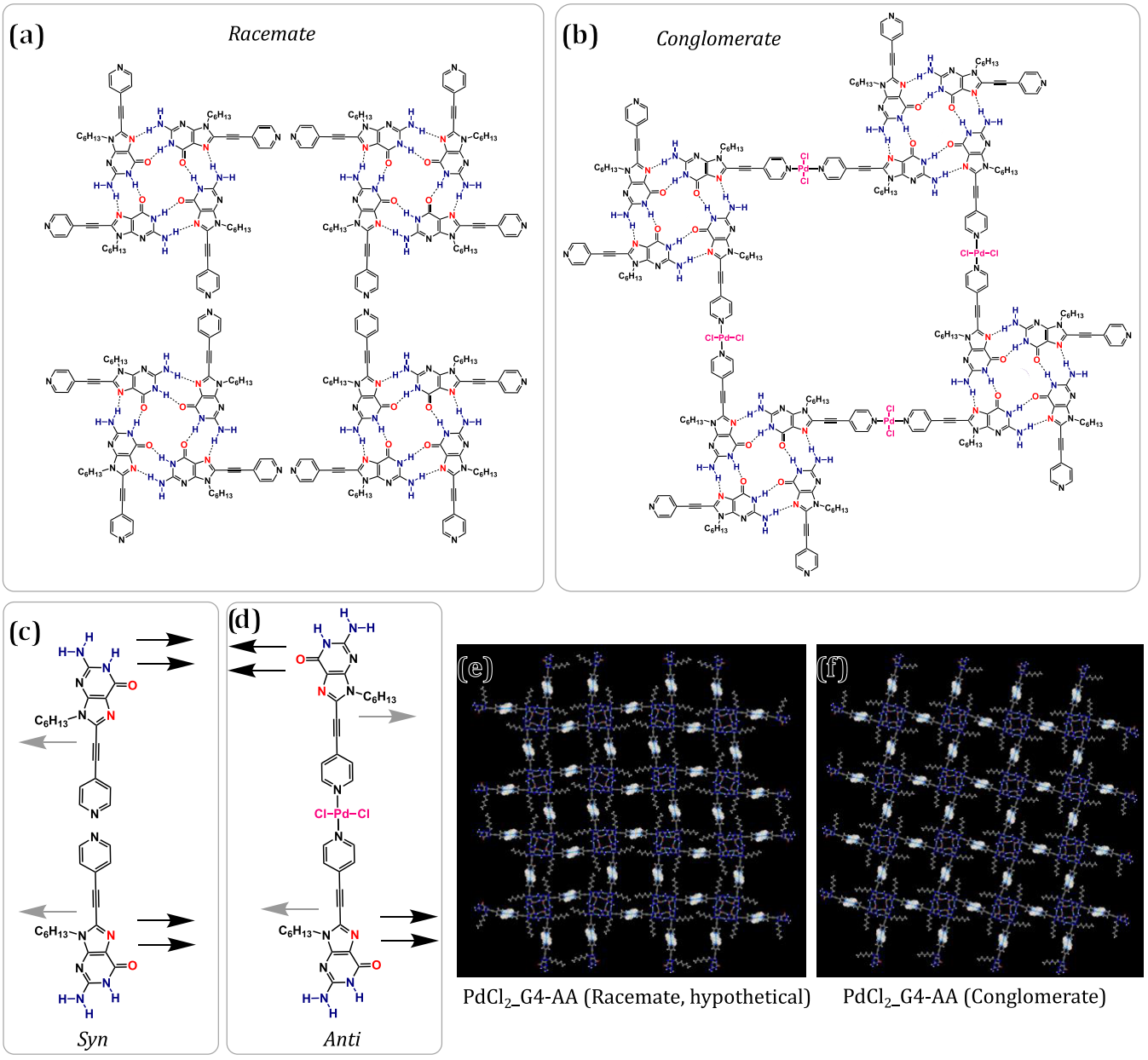

Figure 4. (a, b) Molecular schemes of the racemic compound and the racemic conglomerate, respectively. The guanine molecules in blue highlight the G-quartet arms interacting with each other. (c, d) Molecular scheme showing the syn- and anti-conformations of the surface adsorbed guanine molecules, respectively. Note that the racemic compound is composed exclusively of the syn conformation, whereas the racemic conglomerate is made up of the anti-conformation. (e, f) Simulated molecular models of the metal-coordinated (hypothetical) racemate and experimentally observed conglomerate. Simulations reveal that these two structures are nearly isoenergetic.

The spontaneous resolution could also be achieved when the experiment was carried out using sequential deposition of the Pd(II) salt. Thus, *in situ* addition of $PdCl_2$ dissolved in heptanoic acid/DMSO mixture (0.2% v/v DMSO) to the HOPG substrate containing the racemic compound SAMN of **C6G-4Py** led to the formation of the racemic conglomerate (Figure S4 in the Supporting Information). This indicates that the self-assembling system is sufficiently dynamic under experimental conditions.

Given the porous nature of the SAMNs, host−guest chemistry inside the open cavities was explored. To this end, lead phthalocyanine (PbPc), which has a C_4 symmetry axis perpendicular to the molecular plane, was used as a guest molecule. Figure 3a shows the STM image of the SAMN obtained upon deposition of 1:1 solution containing PbPc and **C6G-4Py** in heptanoic acid. The brighter contrast of the cavities, which shows an approximately square-shaped feature, confirms the adsorption of PbPc within the SAMN. More importantly, the morphology of the host network is reminiscent of the metallosupramolecular network observed upon the addition of the Pd(II). Domains of the opposite-handed G-quartets could be discerned readily indicating that the spontaneous resolution observed upon the addition of Pd(II) could also be achieved upon guest adsorption without the addition of Pd(II). We hypothesize that the square-shaped PbPc acts as a template and thus drives the **C6G-4Py** network into an alternative arrangement involving square-shaped cavities which can only be obtained if the enantiomorphic G-

https://doi.org/10.1021/jacs.2c10933
J. Am. Chem. Soc. 2023, 145, 1194−1205

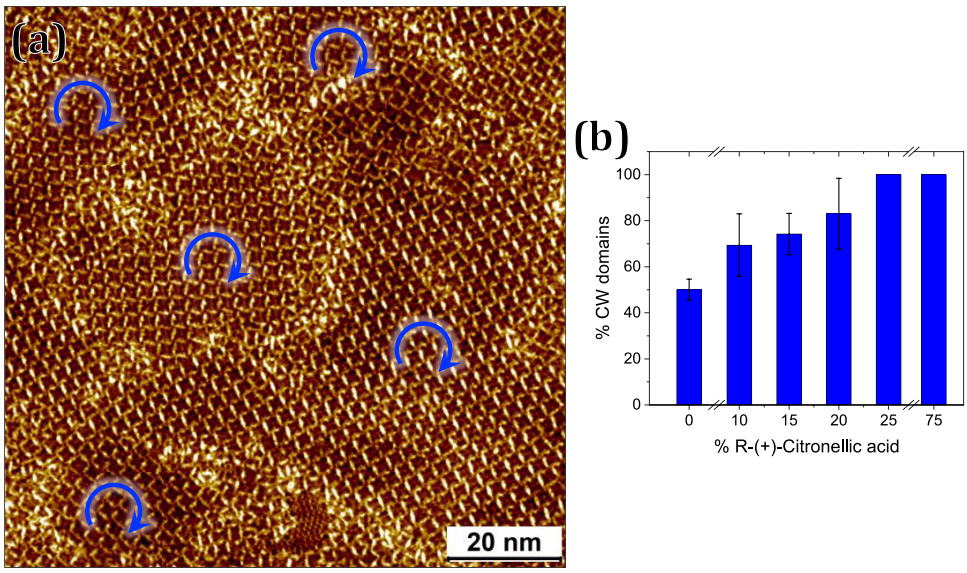

Figure 5. Induction of homochirality in the metallosupramolecular networks of **C6G-4Py** using solvent-mediated chirality transfer. (a) Large-scale STM image of the network obtained upon deposition of a premixed solution of **C6G-4Py** and $PdCl_2$ in (*R*)-(+)-citronellic acid/DMSO 99:1 on HOPG. [**C6G-4Py**] = [$PdCl_2$] = 1.0×10^{-4} M. (b) Variation in the surface coverage of CW G-quartets as a function of volume % of (*R*)-(+)-citronellic acid in a heptanoic acid/(*R*)-(+)-citronellic acid solution mixture. Imaging parameters: (a) I_{set} = 200 pA, V_{bias} = −250 mV. Note that the compact features visible in the lower-middle part of the STM image correspond to the dense self-assembled network formed by **C6G-4Py**. This type of domains were also observed occasionally when the self-assembly of **C6G-4Py** was studied at the heptanoic acid-graphite interface.

quartets are present in separate domains (Figure 3b), thus resulting in a racemic conglomerate. Such guest-mediated spontaneous resolution of racemic compounds into racemic conglomerates has been reported earlier for bulk systems;[62] however, to the best of our knowledge, not in the case of surface-confined MOCNs.

The metalion-mediated spontaneous resolution observed in the current system has not been reported earlier for surface-confined systems and thus merits further scrutiny. To understand the spontaneous resolution, we scrutinize the system on the basis of actual building blocks of the assembly process. Given that guanine-based systems are known to form hydrogen-bonded quartets even in the solution phase,[54] it is not unreasonable to assume that, in the absence of Pd(II), the actual building blocks for the on-surface self-assembly are (partially) H-bonded quartets, whereas in the presence of Pd(II), due to the relatively stronger character of the coordination bond, Pd-coordinated dimers of **C6G-4Py** are expected to be the building blocks of the self-assembly. Furthermore, the dimeric adduct is formed upon encounter of only two molecules *versus* the four needed for the quartet formation. Therefore, if we assume that the formation of the adducts is the preferred event in solution, the orientation of the hydrogen bond acceptor groups in the final MOCN is dictated by their orientation in the adduct.

Continuing the argument further, detailed structural dissection of the racemate and conglomerate networks reveals that, besides the change in the chiral composition and the unit cell of the supramolecular network, addition of Pd(II) changes the manner in which the **C6G-4Py** molecules in adjacent G-quartets are arranged. Figure 4 shows the points of contact between the G-quartets in the case of the racemate (Figure 4a) and the conglomerate (Figure 4b). It can be readily noticed from this schematic that, upon coordination to Pd(II), the anti-adsorption conformation is favored (Figure 4d), whereas in the absence of Pd(II), the G-quartets are adsorbed in a manner such that the "arms" facing each other are adsorbed in a syn conformation (Figure 4c). Based on this structural argument, it is tempting to conclude that the addition of Pd(II) induces an energetic preference such that the Pd-complexed dimers are adsorbed preferentially in the anti-conformation.

To verify if there exists any such preference, the geometry of the metal-coordinated dimer complex was obtained from DFT calculations and imposed in the classical atomistic models *via* the use of harmonic restraints. These calculations revealed that two conformers are isoenergetic and thus there exists no energetic preference for the anti-conformation (see Section 4 in the Supporting Information). Furthermore, preliminary MOCNs models indicate that the experimentally observed, metal-coordinated conglomerate (homochiral at the domain level) and the hypothetical metal-coordinated racemate are essentially isoenergetic. Similarly, early-stage calculations carried out on the metal-free system indicated that there is no obvious energetic preference for the formation of the racemate over conglomerate (see Section 4 in the Supporting Information). These results indicate that the origin of the metalion-mediated spontaneous resolution remains elsewhere. For example, the relative orientation and dynamics of the C_6H_{13} alkyl groups present in the "cavity" between the interacting G-quartets may help stabilize one type of self-assembly (*e.g.*, the conglomerate) over the other (*e.g.*, the racemic compound). The role of excess Pd(II) also needs to be scrutinized in detail.

To achieve homochiral metallosupramolecular monolayers, we resorted to the solvent-mediated chirality transfer approach.[41−44] To this end, self-assembled network formation was studied at the interface between (*R*)-(+)-citronellic acid and graphite. Citronellic acid was chosen due to its structural similarity with the achiral solvent heptanoic acid. Both solvents can interact with the solute molecules *via* hydrogen-bonding and are of comparable length. **C6G-4Py** was dissolved in (*R*)-

https://doi.org/10.1021/jacs.2c10933
J. Am. Chem. Soc. 2023, 145, 1194−1205

(+)-citronellic acid and premixed with a solution of $PdCl_2$ in DMSO. Deposition of the premixed solution onto the graphite surface revealed the formation of a homochiral metallosupramolecular network. Figure 5a shows an STM image depicting the exclusive formation of homochiral domains containing CW G-quartets formed at the (*R*)-(+)-citronellic acid/graphite interface. While some disorder was present, especially at domain borders, formation of CCW G-quartets was never observed when the self-assembly was carried out from (*R*)-(+)-citronellic acid. Furthermore, exclusive formation of CCW G-quartets was observed when the self-assembly was carried out from (*S*)-(−)-citronellic acid (Figure S9 in the Supporting Information).

The extent of chirality induction could be modulated by carrying out the self-assembly from mixtures of heptanoic acid and (*R*)-(+)-citronellic acid. The metal-to-ligand ratio was kept constant. Figure 5b shows the variation in the percentage of CW G-quartets as a function of the percentage of (*R*)-(+)-citronellic acid in the solvent mixture. It is clear that the induction of homochirality is suppressed with an increasing percentage of the achiral solvent in the solvent mixture. This plot also clearly reveals that only 25% (v/v) chiral solvent is necessary to achieve homochirality within the self-assembled metallosupramolecular networks although at 20% (v/v) of the chiral solvent, the efficiency drops to around 80%. The fact that only 25% (v/v) enantiopure solvent is needed for obtaining a homochiral surface indicates that the induction process is relatively more efficient than that reported for alkoxy-substituted dehydrobenzo[12]annulene derivatives[43] and comparable to that observed in the case of 5-(benzyloxy)-isophthalic acid (BIC) derivatives where the chiral solvent is immobilized within the monolayer.[63]

Given the porous nature of the assemblies described here, it is self-evident that the networks are stabilized by (transiently) co-adsorbed solvent molecules. Whether or not the solvent molecules, either heptanoic acid or citronellic acid, are immobilized within the pores on the time scale of STM measurements is not clear. A surprising observation is that when the self-assembly of **C6G-4Py** was carried out from (*R*)-(+)-citronellic acid in the absence of Pd(II), no chiral induction was observed. In fact, the monolayer representative of the racemic compound, similar to that formed at the heptanoic acid-HOPG interface, was observed (Figure S10 in the Supporting Information). This observation clearly indicates that for chiral symmetry breaking to take place, the presence of Pd(II) is necessary, and in the absence of it, both CW and CCW G-quartets are expressed on the surface. Since the C6G-4Py molecule, the Pd(II) coordinated dimer adducts (anti), and the quartets are all prochiral, chiral selection can be exerted at the level of the single molecule or the adduct or the quartet. As (*R*)-(+)-citronellic acid does not induce homochirality in the self-assembled network of **C6G-4Py**, it follows that the enantiopure solvent does not exert any effect on the orientation of the quartets as such and can be interpreted as further evidence of the faster formation of the adducts. On the other hand, the enantioselection observed for the host−guest network indicates that the solvent may be still effective in determining the orientation of the single molecules, which leads eventually to the formation of an enantiopure homochiral host−guest network (Figure S11 in the Supporting Information).

CONCLUSIONS AND OUTLOOK

Coordination-driven chiral self-assembly forms the structural basis of a number of novel materials including chiral 2D-MOFs and 2D MOCNs. Here, we have investigated the emergence and amplification of (homo) chirality in the hybrid 2D MOCNs formed by a prochiral guanine derivative. Using high-resolution STM data, we demonstrate that in the absence of any chiral influence, the guanine derivative forms a monolayer that is representative of a 2D racemate. This system undergoes spontaneous resolution on surface upon coordination to Pd(II) yielding a 2D conglomerate. The chiral symmetry observed in the surface-confined 2D conglomerate could be broken by carrying out the self-assembly from a chiral solvent, which led to the amplification chirality defined by the handedness of the chiral solvent. The solvent-mediated chirality transfer approach used here provides an inexpensive and generic path toward homochiral films of hybrid MOCNs.

While this supramolecularly rich system led to several fascinating experimental observations, a number of structural and mechanistic aspects remain under intense scrutiny in our research group and will be followed up in subsequent work. One of the most interesting and enigmatic aspects is that of the metal-ion-induced spontaneous resolution. Our initial attempts to pinpoint the origin of this fascinating phenomenon have not yielded concrete results yet because the Pd(II) coordinated hypothetical racemate and the experimentally observed conglomerate monolayers were found to be isoenergetic. To gain further insight into the spontaneous resolution process, we have initiated detailed molecular dynamics (MD) simulations including the explicit solvent phase. While these simulations are computationally expensive and slow, we believe that they will provide insight into the role of alkyl chains attached to the guanine units and also into the role of solvent molecules in the stabilization of the experimentally observed networks. Furthermore, the mechanistic aspects of induction of homochirality from enantiopure solvents need to be studied in detail especially since the solvent-mediated chirality transfer does not occur in the absence of added coordinating metal. We strongly believe that a deeper understanding of how chirality is expressed, induced, and relayed within such metal−organic coordination systems will be useful in the rational design of homochiral surfaces based on MOCNs and 2D-MOFs with potential applications in stereoselective guest recognition, sensing, and beyond.

ASSOCIATED CONTENT

Supporting Information

The Supporting Information is available free of charge at https://pubs.acs.org/doi/10.1021/jacs.2c10933.

Experimental materials and methods, details of the molecular mechanics and molecular dynamics simulations, additional and supporting STM data, as well as supporting data from the simulations (PDF)

AUTHOR INFORMATION

Corresponding Authors

Kunal S. Mali − *Division of Molecular Imaging and Photonics, Department of Chemistry, KU Leuven, 3001 Leuven, Belgium;* orcid.org/0000-0002-9938-6446; Email: kunal.mali@kuleuven.be

Steven De Feyter − *Division of Molecular Imaging and Photonics, Department of Chemistry, KU Leuven, 3001*

https://doi.org/10.1021/jacs.2c10933
J. Am. Chem. Soc. 2023, 145, 1194−1205

Leuven, Belgium; orcid.org/0000-0002-0909-9292; Email: steven.defeyter@kuleuven.be

Authors

Antonino Cucinotta − *Division of Molecular Imaging and Photonics, Department of Chemistry, KU Leuven, 3001 Leuven, Belgium*

Christophe Kahlfuss − *CMC UMR 7140, Université de Strasbourg, CNRS, F-67000 Strasbourg, France*

Andrea Minoia − *Laboratory for Chemistry of Novel Materials, Materials Research Institute, University of Mons, 7000 Mons, Belgium*

Samuel Eyley − *Sustainable Materials Lab, Department of Chemical Engineering, KU Leuven, 8500 Kortrijk, Belgium;* orcid.org/0000-0002-1929-8455

Keanu Zwaenepoel − *Division of Molecular Imaging and Photonics, Department of Chemistry, KU Leuven, 3001 Leuven, Belgium*

Gangamallaiah Velpula − *Division of Molecular Imaging and Photonics, Department of Chemistry, KU Leuven, 3001 Leuven, Belgium;* orcid.org/0000-0002-0642-6892

Wim Thielemans − *Sustainable Materials Lab, Department of Chemical Engineering, KU Leuven, 8500 Kortrijk, Belgium;* orcid.org/0000-0003-4451-1964

Roberto Lazzaroni − *Laboratory for Chemistry of Novel Materials, Materials Research Institute, University of Mons, 7000 Mons, Belgium;* orcid.org/0000-0002-6334-4068

Véronique Bulach − *CMC UMR 7140, Université de Strasbourg, CNRS, F-67000 Strasbourg, France*

Mir Wais Hosseini − *CMC UMR 7140, Université de Strasbourg, CNRS, F-67000 Strasbourg, France*

Complete contact information is available at: https://pubs.acs.org/10.1021/jacs.2c10933

Notes

The authors declare no competing financial interest.

■ ACKNOWLEDGMENTS

S.D.F. and K.S.M. gratefully acknowledge financial support from the Fund of Scientific Research Flanders (FWO) and KU Leuven−Internal Funds (C14/19/079). A.C. acknowledges financial support through an FWO Fellowship (1159922N). This work was in part supported by FWO and FNRS under EOS-CHISUB (40007495). The modeling studies are supported by FNRS (CECI, under Grant 2.5020.11) and by Wallonie (ZENOBE Tier-1 facility, grant 1117545). W.T. and S.E. thank Research Foundation Flanders (grant G0A1219N), KU Leuven (grant C14/18/061), and the European Union's European Fund for Regional Development, Flanders Innovation & Entrepreneurship, and the Province of West-Flanders (Accelerate3 project, Interreg Vlaanderen-Nederland program) for financial support. The authors also thank Prof. Yves Geerts (Université Libre de Bruxelles-ULB) for providing purified sample of lead phthalocyanine.

■ REFERENCES

(1) Pilgrim, B. S.; Champness, N. R. Metal-Organic Frameworks and Metal-Organic Cages − A Perspective. *ChemPlusChem* **2020**, *85*, 1842−1856.

(2) Wang, H.; Li, Y.; Li, N.; Filosa, A.; Li, X. Increasing the Size and Complexity of Discrete 2D Metallosupramolecules. *Nat. Rev. Mater.* **2021**, *6*, 145−167.

(3) Winter, A.; Schubert, U. S. Synthesis and Characterization of Metallo-Supramolecular Polymers. *Chem. Soc. Rev.* **2016**, *45*, 5311−5357.

(4) Barth, J. V.; Costantini, G.; Kern, K. Engineering Atomic and Molecular Nanostructures at Surfaces. *Nature* **2005**, *437*, 671−679.

(5) Liu, J.; Abel, M.; Lin, N. On-Surface Synthesis: A New Route Realizing Single-Layer Conjugated Metal−Organic Structures. *J. Phys. Chem. Lett.* **2022**, *13*, 1356−1365.

(6) Griffin, S. L.; Champness, N. R. A Periodic Table of Metal-Organic Frameworks. *Coord. Chem. Rev.* **2020**, *414*, No. 213295.

(7) Zhou, H.-C.; Long, J. R.; Yaghi, O. M. Introduction to Metal−Organic Frameworks. *Chem. Rev.* **2012**, *112*, 673−674.

(8) Chakraborty, G.; Park, I.-H.; Medishetty, R.; Vittal, J. J. Two-Dimensional Metal-Organic Framework Materials: Synthesis, Structures, Properties and Applications. *Chem. Rev.* **2021**, *121*, 3751−3891.

(9) Wang, M.; Dong, R.; Feng, X. Two-Dimensional Conjugated Metal−Organic Frameworks (2D C-MOFs): Chemistry and Function for Moftronics. *Chem. Soc. Rev.* **2021**, *50*, 2764−2793.

(10) Kalenius, E.; Groessl, M.; Rissanen, K. Ion Mobility−Mass Spectrometry of Supramolecular Complexes and Assemblies. *Nat. Rev. Chem.* **2019**, *3*, 4−14.

(11) Dou, J.-H.; Arguilla, M. Q.; Luo, Y.; Li, J.; Zhang, W.; Sun, L.; Mancuso, J. L.; Yang, L.; Chen, T.; Parent, L. R.; et al. Atomically Precise Single-Crystal Structures of Electrically Conducting 2d Metal−Organic Frameworks. *Nat. Mater.* **2021**, *20*, 222−228.

(12) Zhang, Z.; Wang, H.; Wang, X.; Li, Y.; Song, B.; Bolarinwa, O.; Reese, R. A.; Zhang, T.; Wang, X.-Q.; Cai, J.; et al. Supersnowflakes: Stepwise Self-Assembly and Dynamic Exchange of Rhombus Star-Shaped Supramolecules. *J. Am. Chem. Soc.* **2017**, *139*, 8174−8185.

(13) Wang, J.; Zhao, H.; Chen, M.; Jiang, Z.; Wang, F.; Wang, G.; Li, K.; Zhang, Z.; Liu, D.; Jiang, Z.; Wang, P. Construction of Macromolecular Pinwheels Using Predesigned Metalloligands. *J. Am. Chem. Soc.* **2020**, *142*, 21691−21701.

(14) Wiktor, C.; Meledina, M.; Turner, S.; Lebedev, O. I.; Fischer, R. A. Transmission Electron Microscopy on Metal−Organic Frameworks − A Review. *J. Mater. Chem. A* **2017**, *5*, 14969−14989.

(15) Zhu, Y.; Ciston, J.; Zheng, B.; Miao, X.; Czarnik, C.; Pan, Y.; Sougrat, R.; Lai, Z.; Hsiung, C.-E.; Yao, K.; et al. Unravelling Surface and Interfacial Structures of a Metal−Organic Framework by Transmission Electron Microscopy. *Nat. Mater.* **2017**, *16*, 532−536.

(16) Geng, Y.-f.; Li, P.; Li, J.-z.; Zhang, X.-m.; Zeng, Q.-d.; Wang, C. Stm Probing the Supramolecular Coordination Chemistry on Solid Surface: Structure, Dynamic, and Reactivity. *Coord. Chem. Rev.* **2017**, *337*, 145−177.

(17) Dong, L.; Gao, Z. A.; Lin, N. Self-Assembly of Metal−Organic Coordination Structures on Surfaces. *Prog. Surf. Sci.* **2016**, *91*, 101−135.

(18) Garah, M. E.; Ciesielski, A.; Marets, N.; Bulach, V.; Hosseini, M. W.; Samorì, P. Molecular Tectonics Based Nanopatterning of Interfaces with 2D Metal−Organic Frameworks (MOFs). *Chem. Commun.* **2014**, *50*, 12250−12253.

(19) El Garah, M.; Marets, N.; Mauro, M.; Aliprandi, A.; Bonacchi, S.; De Cola, L.; Ciesielski, A.; Bulach, V.; Hosseini, M. W.; Samorì, P. Nanopatterning of Surfaces with Monometallic and Heterobimetallic 1D Coordination Polymers: A Molecular Tectonics Approach at the Solid/Liquid Interface. *J. Am. Chem. Soc.* **2015**, *137*, 8450−8459.

(20) Carvalho, M.-A.; Dekkiche, H.; Nagasaki, M.; Kikkawa, Y.; Ruppert, R. Coordination-Driven Construction of Porphyrin Nanoribbons at a Highly Oriented Pyrolytic Graphite (HOPG)/Liquid Interface. *J. Am. Chem. Soc.* **2019**, *141*, 10137−10141.

(21) Kikkawa, Y.; Nagasaki, M.; Tsuzuki, S.; Fouquet, T. N. J.; Nakamura, S.; Takenaka, Y.; Norikane, Y.; Hiratani, K. Well-Organised Two-Dimensional Self-Assembly Controlled by in Situ Formation of a Cu(II)-Coordinated Rufigallol Derivative: A Scanning Tunnelling Microscopy Study. *Chem. Commun.* **2022**, *58*, 1752−1755.

(22) Li, S.-S.; Northrop, B. H.; Yuan, Q.-H.; Wan, L.-J.; Stang, P. J. Surface Confined Metallosupramolecular Architectures: Formation and Scanning Tunneling Microscopy Characterization. *Acc. Chem. Res.* **2009**, *42*, 249−259.

(23) Shi, J.; Li, Y.; Jiang, X.; Yu, H.; Li, J.; Zhang, H.; Trainer, D. J.; Hla, S. W.; Wang, H.; Wang, M.; Li, X. Self-Assembly of Metallo-Supramolecules with Dissymmetrical Ligands and Characterization by Scanning Tunneling Microscopy. *J. Am. Chem. Soc.* **2021**, *143*, 1224−1234.
(24) Wang, L.; Song, B.; Li, Y.; Gong, L.; Jiang, X.; Wang, M.; Lu, S.; Hao, X.-Q.; Xia, Z.; Zhang, Y.; et al. Self-Assembly of Metallo-Supramolecules under Kinetic or Thermodynamic Control: Characterization of Positional Isomers Using Scanning Tunneling Spectroscopy. *J. Am. Chem. Soc.* **2020**, *142*, 9809−9817.
(25) Mishra, V.; Mir, S. H.; Singh, J. K.; Gopakumar, T. G. Rationally Designed Semiconducting 2d Surface-Confined Metal−Organic Network. *ACS Appl. Mater. Interfaces* **2020**, *12*, 51122−51132.
(26) Sakata, K.; Kashiyama, S.; Matsuo, G.; Uemura, S.; Kimizuka, N.; Kunitake, M. Growth of Two-Dimensional Metal−Organic Framework Nanosheet Crystals on Graphite Substrates by Thermal Equilibrium Treatment in Acetic Acid Vapor. *ChemNanoMat* **2015**, *1*, 259−263.
(27) Kumar, A.; Banerjee, K.; Foster, A. S.; Liljeroth, P. Two-Dimensional Band Structure in Honeycomb Metal−Organic Frameworks. *Nano Lett.* **2018**, *18*, 5596−5602.
(28) Chen, L.-J.; Yang, H.-B.; Shionoya, M. Chiral Metallosupramolecular Architectures. *Chem. Soc. Rev.* **2017**, *46*, 2555−2576.
(29) Gong, W.; Chen, Z.; Dong, J.; Liu, Y.; Cui, Y. Chiral Metal−Organic Frameworks. *Chem. Rev.* **2022**, *122*, 9078−9144.
(30) Xu, Y.; Duan, J.-J.; Yi, Z.-Y.; Zhang, K.-X.; Chen, T.; Wang, D. Chirality of Molecular Nanostructures on Surfaces Via Molecular Assembly and Reaction: Manifestation and Control. *Surf. Sci. Rep.* **2021**, *76*, No. 100531.
(31) Elemans, J. A. A. W.; De Cat, I.; Xu, H.; De Feyter, S. Two-Dimensional Chirality at Liquid-Solid Interfaces. *Chem. Soc. Rev.* **2009**, *38*, 722−736.
(32) Dutta, S.; Gellman, A. J. Enantiomer Surface Chemistry: Conglomerate Versus Racemate Formation on Surfaces. *Chem. Soc. Rev.* **2017**, *46*, 7787−7839.
(33) Yang, B.; Cao, N.; Ju, H.; Lin, H.; Li, Y.; Ding, H.; Ding, J.; Zhang, J.; Peng, C.; Zhang, H.; et al. Intermediate States Directed Chiral Transfer on a Silver Surface. *J. Am. Chem. Soc.* **2019**, *141*, 168−174.
(34) Messina, P.; Dmitriev, A.; Lin, N.; Spillmann, H.; Abel, M.; Barth, J. V.; Kern, K. Direct Observation of Chiral Metal-Organic Complexes Assembled on a Cu(100) Surface. *J. Am. Chem. Soc.* **2002**, *124*, 14000−14001.
(35) Dmitriev, A.; Spillmann, H.; Lingenfelder, M.; Lin, N.; Barth, J. V.; Kern, K. Design of Extended Surface-Supported Chiral Metal-Organic Arrays Comprising Mononuclear Iron Centers. *Langmuir* **2004**, *20*, 4799−4801.
(36) Parschau, M.; Romer, S.; Ernst, K.-H. Induction of Homochirality in Achiral Enantiomorphous Monolayers. *J. Am. Chem. Soc.* **2004**, *126*, 15398−15399.
(37) Tahara, K.; Yamaga, H.; Ghijsens, E.; Inukai, K.; Adisoejoso, J.; Blunt, M. O.; De Feyter, S.; Tobe, Y. Control and Induction of Surface-Confined Homochiral Porous Molecular Networks. *Nat. Chem.* **2011**, *3*, 714−719.
(38) Fasel, R.; Parschau, M.; Ernst, K.-H. Amplification of Chirality in Two-Dimensional Enantiomorphous Lattices. *Nature* **2006**, *439*, 449−452.
(39) Haq, S.; Liu, N.; Humblot, V.; Jansen, A. P.; Raval, R. Drastic Symmetry Breaking in Supramolecular Organization of Enantiomerically Unbalanced Monolayers at Surfaces. *Nat. Chem.* **2009**, *1*, 409−414.
(40) Berg, A. M.; Patrick, D. L. Preparation of Chiral Surfaces from Achiral Molecules by Controlled Symmetry Breaking. *Angew. Chem., Int. Ed.* **2005**, *44*, 1821−1823.
(41) Katsonis, N.; Xu, H.; Haak, R. M.; Kudernac, T.; Tomović, Ž.; George, S.; Van der Auweraer, M.; Schenning, A. P. H. J.; Meijer, E. W.; Feringa, B. L.; De Feyter, S. Emerging Solvent-Induced Homochirality by the Confinement of Achiral Molecules against a Solid Surface. *Angew. Chem., Int. Ed.* **2008**, *47*, 4997−5001.
(42) Destoop, I.; Ghijsens, E.; Katayama, K.; Tahara, K.; Mali, K. S.; Tobe, Y.; De Feyter, S. Solvent-Induced Homochirality in Surface-Confined Low-Density Nanoporous Molecular Networks. *J. Am. Chem. Soc.* **2012**, *134*, 19568−19571.
(43) Destoop, I.; Minoia, A.; Ivasenko, O.; Noguchi, A.; Tahara, K.; Tobe, Y.; Lazzaroni, R.; De Feyter, S. Transfer of Chiral Information from a Chiral Solvent to a Two-Dimensional Network. *Faraday Discuss.* **2017**, *204*, 215−231.
(44) Chen, T.; Yang, W.-H.; Wang, D.; Wan, L.-J. Globally Homochiral Assembly of Two-Dimensional Molecular Networks Triggered by Co-Absorbers. *Nat. Commun.* **2013**, *4*, No. 1389.
(45) Hosseini, M. W. Molecular Tectonics: From Simple Tectons to Complex Molecular Networks. *Acc. Chem. Res.* **2005**, *38*, 313−323.
(46) Hosseini, M. W. Self-Assembly and Generation of Complexity. *Chem. Commun.* **2005**, 5825−5829.
(47) Davis, J. T.; Spada, G. P. Supramolecular Architectures Generated by Self-Assembly of Guanosine Derivatives. *Chem. Soc. Rev.* **2007**, *36*, 296−313.
(48) Phillips, K.; Dauter, Z.; Murchie, A. I. H.; Lilley, D. M. J.; Luisi, B. The Crystal Structure of a Parallel-Stranded Guanine Tetraplex at 0.95å Resolution. *J. Mol. Biol.* **1997**, *273*, 171−182.
(49) Ciesielski, A.; El Garah, M.; Masiero, S.; Samorì, P. Self-Assembly of Natural and Unnatural Nucleobases at Surfaces and Interfaces. *Small* **2016**, *12*, 83−95.
(50) Otero, R.; Schöck, M.; Molina, L. M.; Lægsgaard, E.; Stensgaard, I.; Hammer, B.; Besenbacher, F. Guanine Quartet Networks Stabilized by Cooperative Hydrogen Bonds. *Angew. Chem., Int. Ed.* **2005**, *44*, 2270−2275.
(51) Carpanese, C.; Ferlay, S.; Kyritsakas, N.; Henry, M.; Hosseini, M. W. Molecular Tectonics: Design of 2-D Networks by Simultaneous Use of Charge-Assisted Hydrogen and Coordination Bonds. *Chem. Commun.* **2009**, 6786−6788.
(52) Lackinger, M.; Griessl, S.; Heckl, W. M.; Hietschold, M.; Flynn, G. W. Self-Assembly of Trimesic Acid at the Liquid−Solid Interfacea Study of Solvent-Induced Polymorphism. *Langmuir* **2005**, *21*, 4984−4988.
(53) Seibel, J.; Parschau, M.; Ernst, K.-H. From Homochiral Clusters to Racemate Crystals: Viable Nuclei in 2D Chiral Crystallization. *J. Am. Chem. Soc.* **2015**, *137*, 7970−7973.
(54) Sessler, J. L.; Sathiosatham, M.; Doerr, K.; Lynch, V.; Abboud, K. A. A G-Quartet Formed in the Absence of a Templating Metal Cation: A New 8-(N,N-Dimethylaniline)Guanosine Derivative. *Angew. Chem., Int. Ed.* **2000**, *39*, 1300−1303.
(55) Vidal, F.; Delvigne, E.; Stepanow, S.; Lin, N.; Barth, J. V.; Kern, K. Chiral Phase Transition in Two-Dimensional Supramolecular Assemblies of Prochiral Molecules. *J. Am. Chem. Soc.* **2005**, *127*, 10101−10106.
(56) Viedma, C.; Lennox, C.; Cuccia, L. A.; Cintas, P.; Ortiz, J. E. Pasteur Made Simple − Mechanochemical Transformation of Racemic Amino Acid Crystals into Racemic Conglomerate Crystals. *Chem. Commun.* **2020**, *56*, 4547−4550.
(57) Furukawa, M.; Yamada, T.; Katano, S.; Kawai, M.; Ogasawara, H.; Nilsson, A. Geometrical Characterization of Adenine and Guanine on Cu(110) by NEXAFS, XPS, and DFT Calculation. *Surf. Sci.* **2007**, *601*, 5433−5440.
(58) Poppenberg, J.; Richter, S.; Darlatt, E.; Traulsen, C. H. H.; Min, H.; Unger, W. E. S.; Schalley, C. A. Successive Coordination of Palladium(II)-Ions and Terpyridine-Ligands to a Pyridyl-Terminated Self-Assembled Monolayer on Gold. *Surf. Sci.* **2012**, *606*, 367−377.
(59) Mukherjee, A.; Sanz-Matias, A.; Velpula, G.; Waghray, D.; Ivasenko, O.; Bilbao, N.; Harvey, J. N.; Mali, K. S.; De Feyter, S. Halogenated Building Blocks for 2D Crystal Engineering on Solid Surfaces: Lessons from Hydrogen Bonding. *Chem. Sci.* **2019**, *10*, 3881−3891.
(60) Wallach, O. Zur Kenntniss Der Terpene Und Der Ätherischen Oele. *Justus Liebigs Ann. Chem.* **1895**, *286*, 90−118.

https://doi.org/10.1021/jacs.2c10933
J. Am. Chem. Soc. 2023, 145, 1194−1205

(61) Brock, C. P.; Schweizer, W. B.; Dunitz, J. D. On the Validity of Wallach's Rule: On the Density and Stability of Racemic Crystals Compared with Their Chiral Counterparts. *J. Am. Chem. Soc.* **1991**, *113*, 9811−9820.
(62) Pérez-García, L.; Amabilino, D. B. Spontaneous Resolution under Supramolecular Control. *Chem. Soc. Rev.* **2002**, *31*, 342−356.
(63) Chen, T.; Li, S.-Y.; Wang, D.; Yao, M.; Wan, L.-J. Remote Chiral Communication in Coadsorber-Induced Enantioselective 2D Supramolecular Assembly at a Liquid/Solid Interface. *Angew. Chem., Int. Ed.* **2015**, *54*, 4309−4314.

https://doi.org/10.1021/jacs.2c10933
J. Am. Chem. Soc. 2023, 145, 1194−1205